Vapor Phase Laser Photochemistry and Determination by Electron Diffraction of the Molecular Structure of $[(^tBu)GaS]_4$: Evidence for the Retention of the Ga_4S_4 Cubane Core during the MOCVD Growth of Cubic GaS

William M. Cleaver,[1a] Michael Späth,[1b] Dráhomír Hnyk,[1c,d] Graeme McMurdo,[1c] Michael B. Power,[1a] Michael Stuke,*[,1b] David W. H. Rankin,*[,1c] and Andrew R. Barron*[,1a]

Department of Chemistry, Harvard University, Cambridge, Massachusetts 02138, Max-Planck-Institut für biophysikalische Chemie, Postfach 2841, D-37018 Göttingen, Germany, and Department of Chemistry, University of Edinburgh, West Mains Road, Edinburgh EH9 3JJ, Scotland

Received September 2, 1994[⊗]

The vapor phase structure and decomposition of $[(^tBu)GaS]_4$ have been investigated by gas phase electron diffraction and UV-laser photolysis/time-of-flight mass spectrometry, respectively. The vapor phase structure of $[(^tBu)GaS]_4$, as determined by electron diffraction, consists of a distorted cubane Ga_4S_4 core. Salient structural parameters (r_a) include Ga–S = 2.365(2) Å and Ga–C = 1.976(4) Å. The electron diffraction structure is compared to that determined in the solid state by X-ray diffraction. The gas phase ultraviolet excimer laser-induced photolysis of $[(^tBu)GaS]_4$ has been studied using a photolysis wavelength of 248 nm. The photofragments were detected by laser ionization time-of-flight mass spectroscopy. The formation of photofragments $(^tBu)_xGa_4S_4$ (x = 0–3) is interpreted to indicate the stability of the Ga_4S_4 core. Solid state ablation studies additionally indicate the coupling of two cubane cores. These results are discussed with respect to the metal–organic chemical vapor deposition of the cubic phase of GaS, using $[(^tBu)GaS]_4$ as a single-source precursor.

Introduction

We have recently reported the metal–organic chemical vapor deposition (MOCVD) growth of a new phase of gallium sulfide (GaS) from the single-source precursor compound $[(^tBu)GaS]_4$ (**I**).[2,3] On the basis of electron

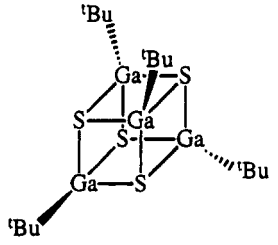

(I)

and X-ray diffraction studies, the new phase was proposed to have a face-centered cubic (*fcc*) structure. This previously unknown cubic phase of GaS has been found to be a suitable material for the electronic passivation[4] of GaAs surfaces.[5,6] In fact, independent theoretical studies have shown it to be the ideal passivation material for GaAs.[7] In addition, the materials large band gap (>3.5 eV) makes it suitable as the insulating "gate" layer in metal–insulator–semiconductor field effect transistor (MISFET)-type devices.[8] Given these fundamental technological developments associated with the new phase of GaS, it is of the utmost importance to understand the growth pathway from a single-source precursor, $[(^tBu)GaS]_4$, to this new solid state phase.

The formation of a meta-stable cubic phase, rather than the thermodynamic hexagonal phase,[9] was shown to be dependent only on the precursor's structure[3] and was rationalized by assuming that the Ga_4S_4 core of the precursor molecule remained intact during deposition and acted as a *predesigned molecular motif* to the solid state phase.[10] As such this system appears to be a rare example of a new solid state material being synthesized by molecular control and represents a unique opportunity for the study of the concept of "molecules to materials".

Evidence for the proposal of molecular control was initially based on electron impact and chemical ionization mass spectral data of the precursor compound,

* Authors to whom correspondence should be addressed.

⊗ Abstract published in *Advance ACS Abstracts*, December 1, 1994.

(1) (a) Harvard University. (b) Max-Planck-Institut für biophysikalische Chemie. (c) University of Edinburgh. (d) On leave from the Institute of Inorganic Chemistry of the Academy of Science of the Czech Republic, 250 68 Řež near Prague, Czech Republic.

(2) MacInnes, A. N.; Power, M. B.; Barron, A. R. *Chem. Mater.* **1992**, *4*, 11.

(3) MacInnes, A. N.; Power, M. B.; Barron, A. R. *Chem. Mater.* **1993**, *5*, 1344.

(4) Passivation is defined as a process that reduces the density of available electronic states present at the surface of a semiconductor, thereby limiting hole and electron recombination possibilities.

(5) MacInnes, A. N.; Power, M. B.; Barron, A. R.; Jenkins, P. P., Hepp, A. F. *Appl. Phys. Lett.* **1993**, *62*, 771.

(6) Tabib-Azar, M.; Kang, S.; MacInnes, A. N.; Power, M. B.; Barron, A. R.; Jenkins, P. P., Hepp, A. F. *Appl. Phys. Lett.* **1993**, *63*, 625.

(7) Medvedev, Yu. V. *Appl. Phys. Lett.* **1994**, *64*, 3458.

(8) Jenkins, P. P.; MacInnes, A. N.; Tabib-Azar, M.; Barron, A. R. *Science* **1994**, *263*, 1751.

(9) (a) Hahn, H. *Angew. Chem.* **1958**, *65*, 538. (b) Kuhn, A.; Chevey, A. *Acta Crystallogr.* **1976**, *B32*, 983.

(10) Barron, A. R. *Comments Inorg. Chem.* **1993**, *14*, 123.

0276-7333/95/2314-0690$09.00/0

Scheme 1. EI Mass Spectral Fragmentation of [(ᵗBu)GaS]₄

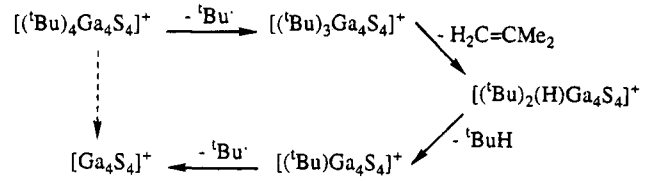

$[(^tBu)GaS]_4$, in which no fragmentation of the Ga_4S_4 core occurs (Scheme 1). However, no direct evidence was available to confirm that the cubane precursor's Ga_4S_4 core was retained through the CVD process, i.e., in the vapor phase during mass transport, during vapor phase decomposition, and on the growth surface. While we cannot, as yet, probe the MOCVD growth surface directly, we have embarked on a program attempting to determine the structure of $[(^tBu)GaS]_4$ under conditions of vapor transport and better understand its decomposition in the vapor phase.

Electron diffraction represents a powerful tool for nondestructive structural determination at high temperatures in the gas phase,[11] allowing for the direct confirmation of the vapor phase structure of $[(^tBu)GaS]_4$. Furthermore, we have previously reported that the UV-excimer laser photolysis of gallium alkyls is an excellent probe of their vapor phase decomposition pathways.[12] The results of our studies in both of these areas are presented herein.

Results and Discussion

Electron Diffraction Studies. While $[(^tBu)GaS]_4$ exhibits volatility at *ca.* 180 °C, during the MOCVD of GaS the vapor transfer lines are held at 220–240 °C to provide saturation of the carrier gas.[13] In order to confirm that $[(^tBu)GaS]_4$ remains intact during vapor phase transport, we determined its structure under analogous temperature conditions.

Using a stainless steel nozzle heated by flowing hot air, we have succeeded in measuring the electron diffraction pattern of $[(^tBu)GaS]_4$ in the vapor phase at 218 °C. The measurements were made at two camera distances, *viz.* 258.6 and 96.6 mm, with an electron wavelength of 0.0569 Å, giving a range of 2–26 $Å^{-1}$ in the scattering variable, s. Three plates were exposed at each camera length.

Given the precedent of the solid state structure,[14] the molecular model of the heavy-atom skeleton of $[(^tBu)GaS]_4$ was based on two penetrating tetrahedra, Ga_4 and S_4, the center of each coinciding with the origin of the coordinate system. C_2 and C_3 symmetry operations were used to generate the appropriate geometry including the position of the *tert*-butyl groups. The structure was thus defined by four bonded distances, r(Ga–S), r(Ga–C), r(C–C), and r(C–H), and by one nonbonded distance, r(Ga···Ga). The Ga–C–C and C–C–H bond angles, as well as the twist angles (τ) of the methyl and *tert*-butyl groups around C–C and Ga–C bonds, were selected to complete the set of nine independent geometrical parameters, as listed in Table 1. The twist angles τ_1 and τ_2 were defined to be zero when the Ga(1)–C(1)–C(11)–H (τ_1) and S(2)–Ga(1)–C(1)–C(11) (τ_2) sets of atoms were coplanar. Values of τ_1 and $\tau_2 < 0$ indicate counterclockwise rotation around the C(1)–C(11) and Ga(1)–C(1) bonds, respectively, viewed from C(1) to C(11) and from Ga(1) to C(1). Overall the molecule had T symmetry. The molecular model for $[(^tBu)GaS]_4$ in its refined form, together with the atomic numbering, is presented in Figure 1.

Table 1. Selected Geometrical Parameters of $[(^tBu)GaS]_4$[a]

p_1	r(Ga···Ga)	3.111(3)	p_6	θ(Ga–C–C)	109.6(4)
p_2	r(Ga–S)	2.365(2)	p_7	θ(C–C–H)	108.0[b]
p_3	r(Ga–C)	1.976(4)	p_8	τ_1(CH_3 twist)	−3.3(2)
p_4	r(C–C)	1.534(3)	p_9	τ_2(CMe_3 twist)	−39.6(1)
p_5	r(C–H)	1.136(7)			

[a] Distances in angstroms and angles in degrees. Figures in parentheses are the estimated standard deviations of the last digits. [b] C–C–H angle fixed for refinement.

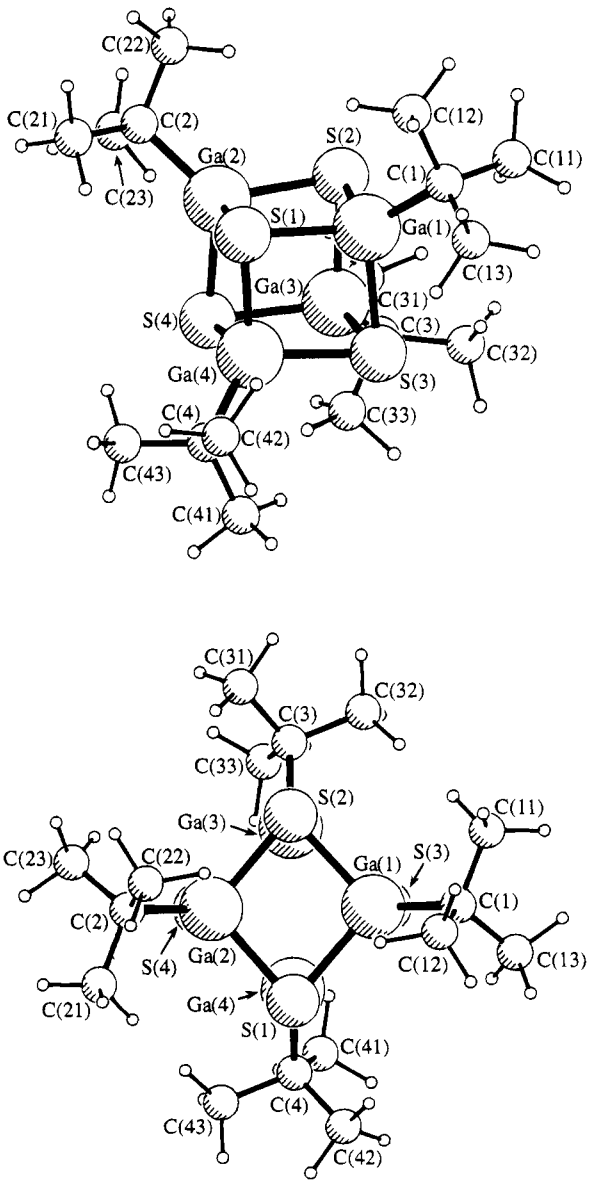

Figure 1. Two perspective views of $[(^tBu)GaS]_4$, together with the atomic numbering, in the optimum refinement of the electron diffraction analysis.

(11) Hargittai, I.; Hargittai, M. *Stereochemical Applications of Gas-Phase Electron Diffraction*; VCH Publishers: New York, 1988.
(12) (a) Cleaver, W. M.; Barron, A. R.; Zhang, Y.; Stuke, M. *Appl. Surf. Sci.* **1992**, *54*, 8. (b) Zhang, Y.; Cleaver, W. M.; Stuke, M.; Barron, A. R. *Appl. Phys. A* **1992**, *55*, 261.
(13) We have previously shown that $[(^tBu)GaS]_4$ shows no decomposition over this temperature range.
(14) Power, M. B.; Barron, A. R. *J. Chem. Soc., Chem. Commun.* **1991**, 1315.

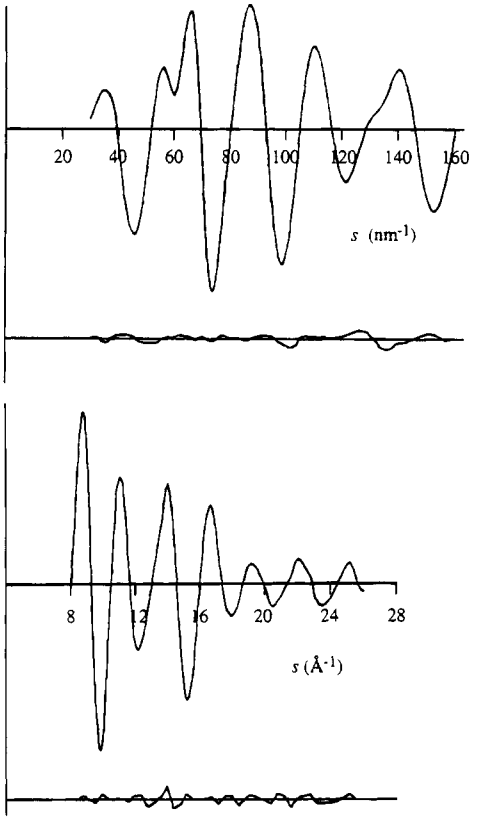

Figure 2. Experimental molecular scattering curves for [(ᵗBu)GaS]$_4$: nozzle-to-plate distances 258.56 (top) and 96.61 mm (bottom).

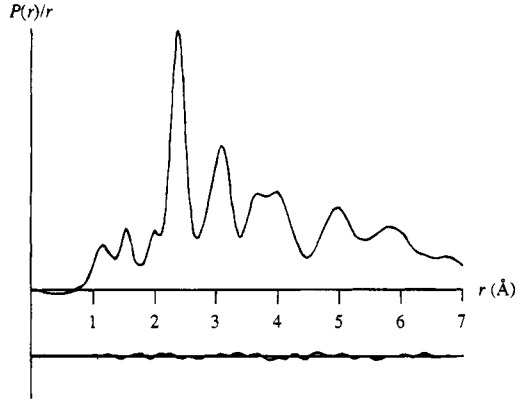

Figure 3. Observed and difference radial distribution curves, $P(r)/r$ against r, for [(ᵗBu)GaS]$_4$. Before Fourier inversion, the data were multiplied by $s \exp(0.002\, s^2)/(Z_{Ga} - f_{Ga})(Z_S - f_S)$.

The experimental molecular scattering curves are shown in Figure 2. The maximum of the short camera distance data had to be limited to $s = 26$ Å^{-1} because it proved to be impossible to obtain high-quality data at high values of the scattering variable, s. Combination of the scaled experimental data sets yielded the radial distribution curve reproduced in Figure 3, which is extraordinarily rich in structural information. The refinement of the geometrical parameters proceeded smoothly; it was possible to refine all the parameters defining the positions of the heavy atoms simultaneously, together with some parameters relating to the positions of the hydrogen atoms. The C–C–H bond angle could not be refined satisfactorily, all such attempts leading to an unreasonably small value (<106°). Both twist angles, τ_1 and τ_2, were also refined, although their values must be considered as "fitting factors" rather than real torsions. This is especially true for τ_1, since the *tert*-butyl methyl groups are undoubtedly mobile due to rotation about the C–C bonds. Table 1 shows the final refined geometrical parameters, while in Table 2 the interatomic distances are listed, along with the values of the corresponding amplitudes of vibration, some of which were coupled and varied in five blocks. The elements of the least-squares correlation matrix exceeding 50% are given in Table 3. Considering the magnitude of the molecule (60 atoms), an excellent agreement between the experimental and computed molecular intensities has been achieved. This optimum refinement corresponds to the value of $R_G = 0.073$ ($R_D = 0.064$).

The cubanelike structure of [(ᵗBu)GaS]$_4$ was found to be distorted from a regular cubic geometry; the Ga–S–Ga angle is decreased to 82.3(1)° and the S–Ga–S angle is increased to 97.3(1)° (see Table 4). Moreover, these rhombohedrally distorted faces are nonplanar with a fold on the diagonal Ga···Ga, of 10.0°. This is clearly significant given that the majority of dimeric gallium compounds are planar. However, it may be compared to the situation of the sulfur atoms in the dimeric thiolate compound [I$_2$Ga(μ-SⁱPr)]$_2$,[15] in which the Ga$_2$S$_2$ ring is in a butterfly geometry with a deviation from planarity of 36.7(2)°.[16] These distortions may be accounted for as follows. First, according to VSEPR theory,[17] the repulsion between the nonbonded electron pair on the sulfide and the Ga–S bonded pairs should be greater than that between the Ga–S bonded pairs themselves. Second, if the geometries of the polyhedra are controlled by packing of the gallium and sulfide ions,[18] then from a consideration of the relative ionic radii for Ga^{3+} (0.62 Å) and the sulfide anion, 1.85 Å, the S···S distance should be longer than the Ga···Ga distance. Both of these explanations would result in a decrease in the Ga–S–Ga bond angle with a concomitant opening of the S–Ga–S bond angle, as is observed experimentally. Similar deformations from the regular cubic structure were observed in the X-ray diffraction studies of the first crystallographically characterized group 13–16 cubane compound, [MeIn(OH)(O$_2$PPh$_2$)]$_4$,[19] as well as the isostructural phosphorus–carbon, [(ᵗBu)CP]$_4$,[20] and arsenic–carbon, [(ᵗBu)CAs]$_4$,[21] cages. As is found for [(ᵗBu)$_2$Ga(μ-SH)]$_2$,[11] [(Ph)$_2$Ga(μ-SEt)]$_2$,[22] and halide-bridged dimers, [R(X)Ga(μ-Cl)]$_2$ (e.g., R = X = Me;[23] R = ᵗBu, X = Cl[24]), the spatial requirements

(15) Hoffmann, G. G.; Burschka, C. *Angew. Chem.* **1985**, *97*, 965; *Angew. Chem., Int. Ed. Engl.* **1985**, *24*, 970.
(16) This distortion has also been observed, in a pentagonal ring, in the thiacarborane, *nido*-7,8,10-C$_2$SB$_8$H$_{10}$, where the B–S–B angle is found to be *ca.* 94°, some 14° less than that for regular C_{5v} symmetry: Hnyk, D.; Hofmann, M.; Schleyer, P. v. R., to be published.
(17) Gillespie, R. J. *Molecular Geometry*, van Nostrand Reinhold: London, 1972.
(18) Mulliken atomic charges from Fenske–Hall calculations revealed the [(ᵗBu)GaS]$_4$ clusters to be fairly ionic. The charges on each S and Ga atom are −0.75 and +1.20, respectively: Subramanian, L.; Lichtenberger, D. L.; Power, M. B.; Barron, A. R., unpublished results.
(19) Arif, A. M.; Barron, A. R. *Polyhedron* **1988**, *7*, 2091.
(20) Wettling, T.; Schneider, J.; Wagner, O.; Kreiter, C. G., Regitz, M. *Angew. Chem., Int. Ed. Engl.* **1989**, *32*, 1013.
(21) Hitchcock, P. B.; Johnson, J. A.; Nixon, J. F. *Angew. Chem., Int. Ed. Engl.* **1993**, *27*, 103.
(22) Hoffman, G. G.; Burschlea, C. *J. Organomet. Chem.* **1984**, *267*, 229.

Table 2. Interatomic Distances (r_a, Å)[a] and Mean Amplitudes of VIbration (u, Å) for [(ᵗBu)GaS]₄

atomic pair	r_a[b]		u[b]	key to coupling scheme
Ga−S	2.365(2)	u_1	0.085(3)	
Ga−C	1.976(4)	u_2	0.047(6)	
C−C	1.534(3)	u_3	0.049(5)	
C−H	1.136(7)	u_4	0.085(7)	
Ga···Ga	3.111(3)	u_5	0.123(4)	
S···S	3.550(6)	u_6	0.110(7)	
Ga···S	4.079(4)	u_7	0.097(6)	
Ga(1)···C(11)	2.880(5)	u_8	0.114(8)	
Ga(1)···C(2)	4.861(5)	u_9	0.150(10)	
Ga(1)···C(21)	5.613(10)[c]	u_{10}	0.225(18)	i
Ga(1)···C(22)	5.076(9)[c]	u_{11}	0.236(8)	ii
Ga(1)···C(23)	5.885(9)[c]		0.225	i
S(1)···C(1)	3.764(4)	u_{12}	0.140(22)	
S(4)···C(1)	6.055(5)	u_{13}	0.155(3)	iii
S(1)···C(11)	5.032(6)[c]		0.189	ii
S(2)···C(11)	3.900(11)[c]		0.104[d]	
S(3)···C(11)	4.334(15)[c]	U_{14}	0.190(19)	
S(4)···C(11)	6.727(8)	u_{15}	0.229(18)	iv
C(1)···C(2)	6.338(8)		0.194	iii
C(1)···C(21)	7.045(15)[c]		0.160[d]	
C(1)···C(22)	6.160(11)[c]		0.194	iii
C(1)···C(23)	7.483(12)[c]		0.230[d]	
C(11)···C(12)	2.502(8)	u_{16}	0.086(26)	
C(11)···C(21)	7.984(27)[c]	u_{17}	0.263(38)	v
C(11)···C(22)	6.730(22)[c]		0.229	iv
C(11)···C(23)	8.009(12)[c]		0.263	v
C(12)···C(23)	7.460(21)[c]		0.230[d]	
C(12)···C(22)	5.705(26)[c]		0.225	i
C(13)···C(23)	8.662(16)[c]		0.190[d]	

[a] The Ga···H, S···H, C···H, and H···H nonbonded distances were included in the refinement, but they are not listed here. Their vibrational amplitudes were within the range 0.104−0.35 Å. [b] Least-squares standard deviations in the last digit are given in parentheses. [c] Dependent on the $C(CH_3)_3$ twist angle (τ_2). [d] Fixed.

Table 3. Analysis of the Electron Diffraction Pattern of [(ᵗBu)GaS]₄: Portion of the Least-Squares Correlation Matrix Listing Off-Diagonal Elements (×100) with Absolute Values ≥50%[a]

u_1	u_8	u_{10}	u_{12}	u_{13}	u_{15}	u_{16}	k_1	k_2	
79			65			93	58	65	p_2
		65		57					p_8
					52				p_9
			57			86	85	79	u_1
	75								u_5
			74						u_6
						63	51	59	u_{12}
		75							u_{13}
							65	71	u_{16}
								79	k_1

[a] k_1 and k_2 are scale factors.

of the sulfide anion results in a large Ga···Ga nonbonded distance across the Ga_2S_2 face (Table 4). This is in contrast to the values observed for hydride-bridged species (2.58−2.61 Å).[25]

It has been previously reported[26] that the solid state structures of several transition metal−chalcogenide cubane clusters, e.g., $[(X)FeS]_4^{n-}$, show distortion due to crystal packing forces. However, no direct comparison with a vapor phase system has been available. It is useful, therefore, to compare the electron diffraction structure obtained in the present work with that obtained previously by single-crystal X-ray diffraction techniques (see Table 4).[14] It is clear from Table 4 that all the chemically equivalent parameters are within experimental error the same. This suggests that the Ga_4S_4 core structure is sufficiently robust to be unaffected by any crystal-packing forces. Furthermore, the cores appear to be invariant over a significant temperature range, −90 to 220 °C.

Table 4. Comparison of Bond Lengths (Å) and Angles (deg) in [(ᵗBu)GaS]₄ As Determined by Electron Diffraction (ED) and X-Ray Diffraction (XRD)

parameter	ED	XRD[a]
Ga−S	2.365(2)	2.359(3)
Ga−C	1.976(4)	1.978(6)
Ga···Ga	3.111(3)	3.100(6)
S···S	3.550(6)	3.544(6)
S−Ga−S	97.3(1)	97.3(1)
Ga−S−Ga	82.3(1)	82.1(1)

[a] Power, M. B.; Barron, A. R. *J. Chem. Soc., Chem. Commun.* **1991**, 1315.

Vapor Phase Photolysis of [(ᵗBu)GaS]₄. It has been previously demonstrated that the gas phase infrared laser powered homogeneous pyrolysis (IR-LPHP) of group 13 organometallics closely mimics the decomposition that occurs under MOCVD conditions.[27] Attempts to study the gas phase decomposition of [(ᵗBu)GaS]₄ using IR-LPHP was precluded by the compound's limited volatility.[28] However, we have shown that under certain conditions the UV photochemical decomposition pathways for gallium alkyls follows that of their thermolysis.[12]

For any organometallic to be suitable for photolytic decomposition, it must absorb in the UV (or visible) at a wavelength corresponding to common laser or arc lamp emissions; for example, 193 (ArF excimer laser), 248 (KrF excimer laser), or 308 nm (XeCl excimer laser) would be desirable. Due to experimental difficulties in determining the vapor phase UV absorption spectrum of [(ᵗBu)GaS]₄, and since we have previously shown that the UV−visible spectrum of gallium alkyls in hydrocarbon solution is identical to that observed in the vapor phase,[12,29] the solution spectrum of [(ᵗBu)GaS]₄ was determined and is shown in Figure 4. The molar absorption coefficient (ϵ = 300 L.mol^{-1}cm^{-1}) of the major absorption at 220 nm is comparable to those previously measured for $GaMe_3$, $Ga(^tBu)Me_2$, and $Ga(^tBu)_2Me$.[29] Based on the UV spectrum of [(ᵗBu)GaS]₄ and our previous studies[12] a UV-excimer laser (248 nm) was chosen for photolysis.

To create and detect the various gallium containing photo products a TOF mass spectrometer[30] was equipped with a sample holder and quartz windows for two opposing collinear laser beams for photolysis and ionization. A schematic of the experimental apparatus is given in Figure 5.[31] The first UV-excimer laser (248 nm) photolyzes the precursor into neutral fragments. The second UV-excimer laser (248 nm), delayed by 0.4−0.5 μs, ionizes the photofragments. The ions are then accelerated in the mass spectrometer, and depending on the time of flight (TOF) of the accelerated ion, the

(23) Baxter, P. L; Downs, A. J.; Goode, M. J.; Rankin, D. W. H.; Robertson, H. E. *J. Chem. Soc., Dalton Trans.* **1990**, 2873.
(24) Power, M. B.; Cleaver, W. M.; Apblett, A. W.; Barron, A. R.; Ziller, J. W. *Polyhedron* **1992**, *11*, 477.
(25) Pulham, C. R.; Downs, A. J.; Goode, M. J.; Rankin, D. W. H.; Robertson, H. E. *J. Am. Chem. Soc.* **1991**, *113*, 5149.
(26) Snyder, B. S.; Holm, R. H. *Inorg. Chem.* **1988**, *27*, 2339, and references therein.
(27) Russel, D. K. *Coord. Chem. Rev.* **1992**, *112*, 131.
(28) Russell, D. K.; Barron, A. R., unpublished results.
(29) Cleaver, W. M.; Barron, A. R. Chemtronics **1989**, *4*, 146.
(30) Stuke, M. *Appl. Phys. Lett.* **1984**, *45*, 1175.
(31) Larciprete, R.; Stuke, M. *J. Phys. Chem.* **1986**, *90*, 4568.

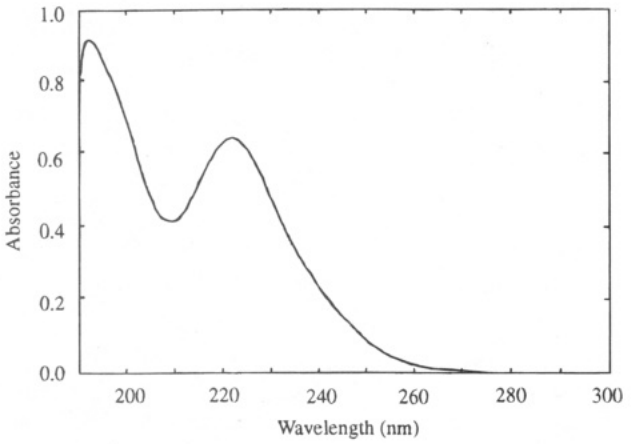

Figure 4. Solution UV−visible spectrum of $[(^t\text{Bu})\text{GaS}]_4$ (λ_{max} = 222 nm, ϵ = 300 L mol^{-1}cm^{-1}).

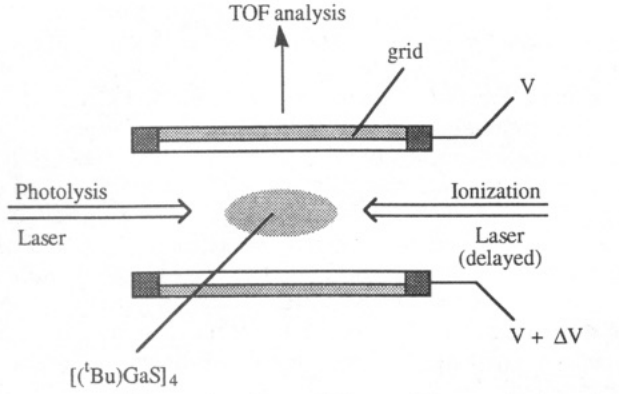

Figure 5. Schematic view of the collinear photolysis/ionization laser arrangement used to study the vapor phase photolysis of $[(^t\text{Bu})\text{GaS}]_4$.

mass can be determined (see Experimental Section). Variation of the source temperature was used to control the pressure of the vapor in the photolysis/ionization chamber. TOF mass spectra were as expected found to be essentially independent of pressure over the range 5.5×10^{-7}–1.7×10^{-6} mbar.

In order to separate the effects of the fragmentation and ionization laser sources, the laser fluence of the fragmentation laser was reduced. In a similar manner, the focus of the ionization source was systematically varied until ion fragmentation was minimized. Thus, the photochemical fragmentation was determined by collection of the TOF mass spectra obtained by photolysis only, ionization only, and both photolysis and ionization (see Figure 6).

The TOF mass spectrum obtained upon UV-excimer laser photolysis (in the absence of ionization laser irradiation) of $[(^t\text{Bu})\text{GaS}]_4$ vapor only shows peaks due to the dimethylcarbene ion $[C(CH_3)_2]^+$ (m/z = 42) and the methylcarbyne ion $[C(CH_3)]^+$ (m/z = 27); see Figure 6 (lower trace). However, their low intensity precludes any definitive discussion of their source. The major peak in the TOF mass spectrum of $[(^t\text{Bu})\text{GaS}]_4$ vapor, without prior photolysis, is that of the parent ion, $[(^t\text{Bu})_4\text{Ga}_4\text{S}_4]^+$ (m/z = 636, 100%). Subsequent peaks due to $[(^t\text{Bu})_3\text{Ga}_4\text{S}_4]^+$ (m/z = 579, 14%), $[(^t\text{Bu})_2\text{Ga}_4\text{S}_4]^+$ (m/z = 522, 5%), and $[C(CH_3)_3]^+$ (m/z = 57) are seen (see Figure 6, middle trace) in agreement with our previous 70 eV EI mass spectral data. From the upper trace in Figure 6 it can be seen that a combination of

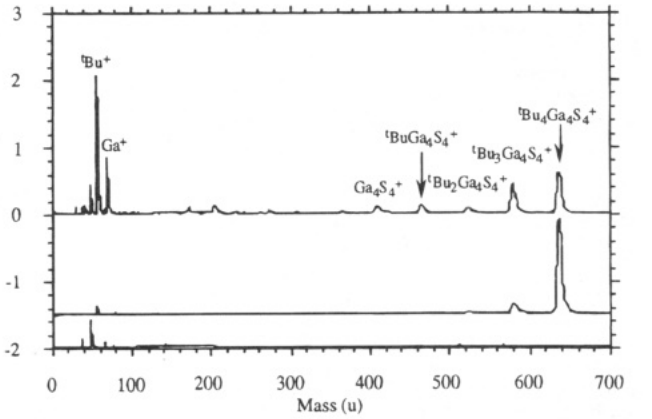

Figure 6. Traces for the time-of-flight mass spectra obtained for $[(^t\text{Bu})\text{GaS}]_4$, using the photolysis laser only (lower trace), the ionization laser only (middle trace) and both photolysis and ionization lasers (upper trace).

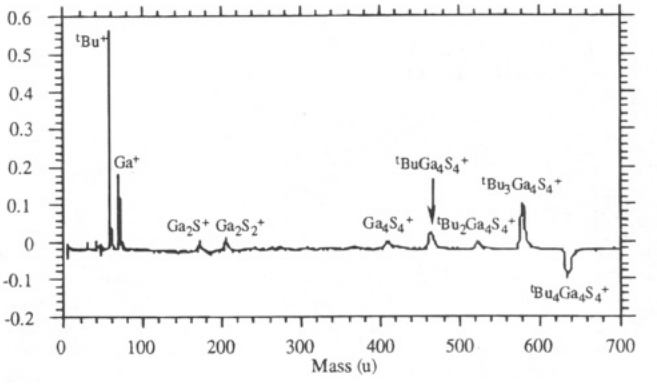

Figure 7. Difference trace for the TOF mass spectra of the photolysis laser only and the ionization laser only subtracted from the spectrum of $[(^t\text{Bu})\text{GaS}]_4$, obtained by use of both the photolysis and ionization lasers.

photolysis and ionization results in the significant enhancement of the $[(^t\text{Bu})_3\text{Ga}_4\text{S}_4]^+$, $[(^t\text{Bu})_2\text{Ga}_4\text{S}_4]^+$, and $[C(CH_3)_3]^+$ peaks. However, additional major peaks due to $[(^t\text{Bu})\text{Ga}_4\text{S}_4]^+$ (m/z = 465) and $[\text{Ga}_4\text{S}_4]^+$ (m/z = 419), as well as $^{69}\text{Ga}^+$ and $^{71}\text{Ga}^+$ ions, are also observed. The only other peaks that can be readily assigned are due to $[\text{Ga}_2\text{S}]^+$ (m/z = 170) and $[\text{Ga}_2\text{S}_2]^+$ (m/z = 202).

Subtraction of the photolysis-only and ionization-only spectra from the combination spectrum in Figure 6 results in a difference spectrum, Figure 7, in which positive (upward) peaks indicate an increase in the fragment upon photolysis, while negative (downward) peaks indicate a decrease in the abundance of a fragmentation product.

Based upon Figure 7, several observations may be made. First, the most obvious result of UV photolysis on $[(^t\text{Bu})\text{GaS}]_4$ vapor is the decrease in intensity of the parent ion and a concomitant increase in the intensity of the trialkyl fragment, $[(^t\text{Bu})_3\text{Ga}_4\text{S}_4]^+$, consistent with the photochemical bond homolysis of one Ga−C bond, eq 1, as the major photochemical reaction. Second, the

$$[(^t\text{Bu})\text{GaS}]_4 \xrightarrow{h\nu\ (248\ \text{nm})} [(^t\text{Bu})_3\text{Ga}_4\text{S}_4] + {}^t\text{Bu}^\bullet \quad (1)$$

relative intensity of the subsequent products due to loss of two, three, and four *tert*-butyl groups is independent of parent ion fragmentation, i.e., that of decreasing intensity with decreasing mass. The $[(^t\text{Bu})\text{Ga}_4\text{S}_4]^+$ ion is more abundant than the $[(^t\text{Bu})_2\text{Ga}_4\text{S}_4]^+$ ion. This

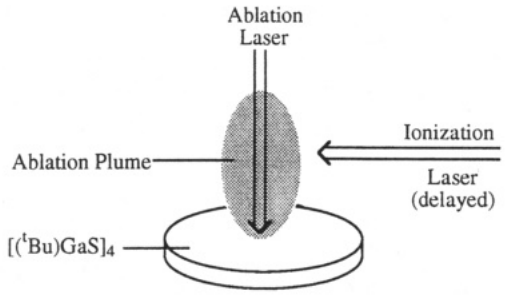

Figure 8. Schematic view of the setup used for the laser ablation of $[(^tBu)GaS]_4$.

suggests that $[(^tBu)_3Ga_4S_4]^+$ may undergo a second photochemical fragmentation, eq 2, since a similar two-

$$[(^tBu)_3Ga_4S_4] \xrightarrow{h\nu\,(248\ nm)} [(^tBu)Ga_4S_4] + 2{}^tBu^\bullet \quad (2)$$

$$GaMe_3 \xrightarrow{h\nu\,(\lambda < 250\ nm)} GaMe + 2Me^\bullet \quad (3)$$

alkyl elimination reaction has been shown to occur for $GaMe_3$ upon photolysis at wavelengths below 250 nm, eq 3.[32] N. B. the absence of $[(CH_3)_3CC(CH_3)_3]^+$ as a photo-fragment precludes reductive elimination of the two *tert*-butyl groups as a pathway, assuming that all alkane fragments are ionized. Third, the presence of core fragmentation peaks, $[Ga_2S]^+$ and $[Ga_2S_2]^+$, as well as Ga atoms, suggests that under the conditions of the present experiment the Ga_4S_4 core undergoes some fission (see below). Besides which the Ga_4S_4 core is clearly retained as the major fragment.

Laser Ablation of $[(^tBu)GaS]_4$. Considering that under thermal MOCVD conditions the precursor may initiate decomposition either in the gas phase or on the substrate surface, we investigated the photolysis of $[(^tBu)GaS]_4$ in the solid state as a simple model for surface decomposition.

A pellet (0.5 cm diameter) of $[(^tBu)GaS]_4$ was prepared in a 2 ton press and mounted on a platform within the TOF mass spectrometer. A 248 nm UV-excimer laser oriented perpendicular to the surface of the sample and another pulsed UV laser parallel to and above the surface were used as the ablation and ionization lasers, respectively. A schematic of the experimental arrangement is shown in Figure 8.

As with the vapor phase photolysis experiments described above, a background TOF mass spectrum was collected using the ionization laser only. As can be seen from the lower trace in Figure 10, the only significant peaks observed were that of the parent ion, and the major ionization fragmentation product, $M^+ - {}^tBu$ (see above). The presence of this signal suggests that $[(^tBu)GaS]_4$ is sufficiently volatile (at 25 °C, 1.7×10^{-6} mbar) to provide a significant vapor phase concentration above the solid sample.

The TOF mass spectrum obtained upon UV-excimer laser ablation of $[(^tBu)GaS]_4$ is shown in the upper traces in Figures 9 and 10. While, from Figure 10, it is clear that the parent ion peak is significantly increased in intensity it is worth noting the presence of fragments due to successive loss of *tert*-butyl, i.e., $[(^tBu)_xGa_4S_4]^+$ ($x = 1-3$). Related to this observation, the major

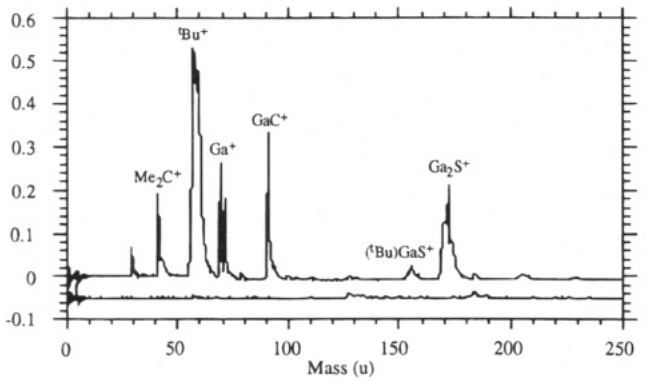

Figure 9. TOF mass spectra (0–250 amu) obtained for the laser ablation of $[(^tBu)GaS]_4$, using the ionization laser only (lower trace) and both the ablation and ionization lasers (upper trace).

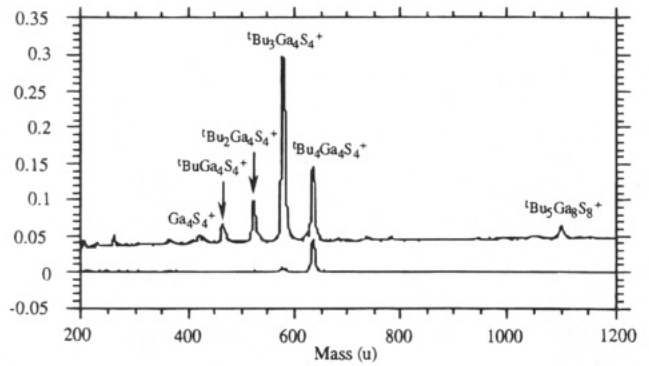

Figure 10. TOF mass spectra (200–1200 amu) obtained for the laser ablation of $[(^tBu)GaS]_4$, using the ionization laser only (lower trace) and both the ablation and ionization lasers (upper trace).

fragmentation peak upon ablation is that of the *tert*-butyl radical, consistent with Ga–C bond cleavage, a process obviously related to the MOCVD process (see Scheme 1). Additional peaks are seen due to the dimethyl-carbene ion $[C(CH_3)_2]^+$ and the methylcarbyne ion $[C(CH_3)]^+$, possibly as fragmentation products of *tert*-butyl groups. The peaks at masses 56 and 91 were determined to be background. These results are supportive of the vapor phase experiments (see above). However, two features are different in the TOF mass spectrum of laser-ablated $[(^tBu)GaS]_4$ as compared to the analogous vapor phase photolysis.

Whereas the vapor phase photolysis of $[(^tBu)GaS]_4$ shows some fragmentation of the cubane core as indicated from the presence of $[Ga_2S]^+$ (*ca.* 3%) and $[Ga_2S_2]^+$ (*ca.* 5%), the intensity of the former is greatly enhanced (40%) during laser ablation. In fact, the peak is comparable in intensity to that of $[(^tBu)_3Ga_4S_4]^+$. The source of $[Ga_2S]^+$ may be twofold. First, under ablation conditions the solid state photolysis of $[(^tBu)GaS]_4$ may yield more Ga_4S_4 core fragmentation. Alternatively, laser ablation may involve significant decomposition of $[(^tBu)GaS]_4$ to GaS. Supporting evidence for this process may be obtained from the TOF mass spectrum obtained from laser ablation of a sample of MOCVD grown cubic GaS, in which $[Ga_2S]^+$ and $[Ga_2S_2]^+$ are the major sulfur-containing fragments observed.

In the vapor phase photolysis mass spectrum the largest peak observed was that of the parent ion $[(^tBu)_4Ga_4S_4]^+$. In contrast, ablation of $[(^tBu)GaS]_4$ in the solid state allows for the observation of an octameric

(32) Zhang, Y.; Beuermann, Th.; Stuke, M. *Appl. Phys. B* **1989**, *48*, 97.

fragment, $[(^tBu)_5Ga_8S_8]^+$ (m/z = 1093, 3%). We have previously observed that the solution thermolysis of $[(^tBu)GaS]_4$ in pentane yields the octameric cage compound $[(^tBu)GaS]_8$ in low yield.[33,34] However, the mass spectrum of $[(^tBu)GaS]_8$, like that of all the gallium sulfide clusters $[(^tBu)GaS]_n$, shows the parent ion with the only significant fragmentation being loss of a single *tert*-butyl group. Thus, it is unlikely that the peak at m/z = 1093 is due to the formation of $[(^tBu)GaS]_8$. Instead we tentatively propose that the $[(^tBu)_5Ga_8S_8]^+$ fragment is the $M^+ - {}^tBu$ fragment of $[(^tBu)_6Ga_8S_8]$ (**II**)

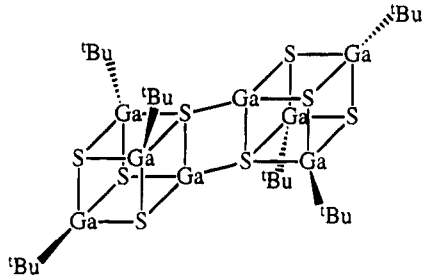

(II)

formed as a result of the coupling of two $[(^tBu)_3Ga_4S_4]$ units, clearly a process related to the growth of GaS thin films. We note, however, that without more in-depth studies it is not possible to establish where the dimerization event occurs: in the gas phase, in the plume, or in a subsequent cooled region of the expanded gas.

Conclusions

The vapor phase structure and decomposition of $[(^tBu)GaS]_4$ have been investigated by gas phase electron diffraction and UV-laser photolysis/time-of-flight mass spectrometry, respectively. By the use of gas phase electron diffraction we have determined that the Ga_4S_4 core of the cubane single-source precursor compound, $[(^tBu)GaS]_4$, remains intact under the conditions employed for vapor transport during the MOCVD growth of cubic GaS. In addition, the similarity of the core structures between the solid state (at −90 °C) and the gas phase (at 220 °C) attests to the high stability of the gallium−sulfide cubane core. Further evidence for the retention of the Ga_4S_4 core during the MOCVD growth of GaS films is obtained from vapor phase UV-laser photolysis/time-of-flight mass spectrometry, where the major photofragmentation is due to loss of the organic substituents *without core cleavage*, i.e., $[(^tBu)_x$-$Ga_4S_4]^+$ (x = 1−3). The coupling of two cubane cores is observed to occur during the laser ablation of a solid sample of $[(^tBu)GaS]_4$, suggestive of the growth of GaS films via the oligomerization of Ga_4S_4 subunits. We are at present attempting to study the surface decomposition of $[(^tBu)GaS]_4$ under UHV conditions, thus completing the cycle of molecular precursor to solid state material.

Experimental Section

General Procedures. $[(^tBu)GaS]_4$ was prepared according to previously published procedures,[35] and was purified by sublimation (170 ° C, at 10^{-2} mmHg). Measurement of the parent molecular ion by ultrashort laser mass spectroscopy[36] confirmed the purity. The solution UV spectrum was measured with a Perkin Elmer Lambda 4C UV/Vis spectrometer in hexane solution.

Table 5. Selected Electron Diffraction Data Collection Parameters for $[(^tBu)GaS]_4$

	nozzle-to-plate distance (mm)	
	258.56	96.61
weighting functions (Å^{-1})		
Δs	0.2	0.4
s_{min}	3.0	8.0
sw_1	5.0	10.0
sw_2	13.6	22.0
s_{max}	16.0	26.0
correlation parameter, p/h	0.4858	−0.1501
scale factor,[a] k	0.700(21)	0.559(20)
electron wavelength[b] (Å)	0.05690	0.05692

[a] Figures in parentheses are the estimated standard deviations of the last digits. [b] Determined by reference to the scattering pattern of benzene vapor.

Electron Diffraction. The electron diffraction patterns for $[(^tBu)GaS]_4$ were recorded photographically on Kodak Electron Image plates using the Edinburgh gas diffraction apparatus.[37] The sample was held at 216 °C during the experiments, and the stainless steel nozzle was held at 218 °C. Three plates at the long camera distance and three at the short distance were used, and plates were also obtained for benzene, under the same experimental conditions, to provide calibration of the electron wavelength. Plates were traced using a Joyce-Loebl Microdensitometer 6[38] at the Daresbury laboratory of the Science and Engineering Research Council.

The scattering data were analyzed using the data reduction[39] and least-squares refinement[39] programs described previously, with the electron scattering factors taken from ref 40. The weighting points needed to set up the off-diagonal weight matrices used in the least-squares refinements are listed in Table 5, together with other experimental parameters. The molecular scattering intensity curves are shown in Figure 2, and the radial distribution curve is given in Figure 3. Refined geometrical parameters are listed in Table 1, interatomic distances and amplitudes of vibration in Table 2, and the most significant elements of the least-squares correlation matrix in Table 3.

Time-of-Flight Mass Spectroscopy. A schematic of the experimental setup to measure the photoproducts is shown in Figure 11. The vacuum system (capable of UHV) consists of a main chamber, into which the sample is introduced by a molecular leak valve. The laser beam enters through a Suprasil quartz window after passing a variable attenuator and a spherical focusing lens with f = 250−500 mm. The focal intensity is in the range of megawatts to several gigawatts per square centimeter. Ions generated in the focus of the laser beam(s) are slightly pushed (*ca.* 100 V cm^{-1}) and accelerated (*ca.* 2000 V) before they drift through the field-free section in the differentially pumped (*ca.* 10^{-8} Torr) side arm, serving as the TOF mass analyzer. The ions are detected by a tandem channel plate detector, and the resulting signal is preamplified and transferred to a transient recorder (Tektronix 7612 D), which can store the complete mass spectrum

(33) Power, M. B.; Ziller, J. W.; Barron, A, R. *Organometallics* **1992**, *11*, 2783.

(34) Similar coupling of clusters has been observed for fullerenes; see: Whetten, R. L.; Jeretzian, C. *Clusters and Fullerenes*; World Scientific Publishing: London, 1993; p 226.

(35) Power, M. B.; Ziller, J. W.; Tyler, A. N.; Barron, A. R. *Organometallics* **1992**, *11*, 1055.

(36) Larciprete, R.; Stuke, M. *J. Cryst. Growth*, **1986**, *77*, 235.

(37) Huntley, C. M.; Laurenson, G. S.; Rankin, D. W. H. *J. Chem. Soc., Dalton Trans.* **1980**, 954.

(38) Cradock, S.; Koprowski, J.; Rankin, D. W. H. *J. Mol. Struct.* **1981**, *71*, 113.

(39) Boyd, A. S. F.; Laurenson, G. S.; Rankin, D. W. H. *J. Mol. Struct.* **1981**, *71*, 217.

(40) Ross, A. W.; Fink, M.; Hilderbrandt, R. In *International Tables for X-ray Crystallography*; Volume C, Wilson, A. J. C., Ed.; Kluwer Academic Publishers: Boston, 1992; p 245.

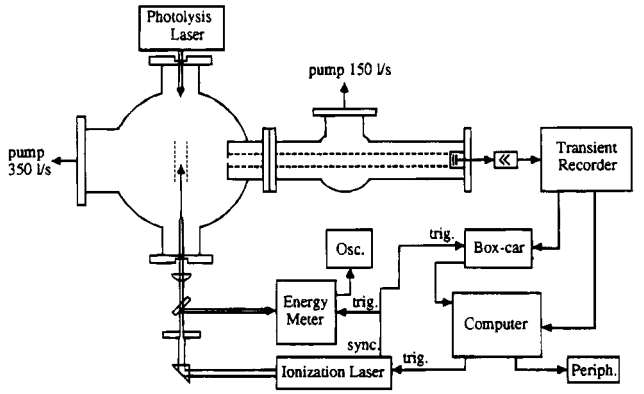

Figure 11. Schematic of the experimental setup[26] with UV-excimer lasers for photolysis and ionization for detection on perpendicular axes; *cf.* Figure 5.

for each laser shot. Data are transferred to a Macintosh computer, which also triggers the ionization laser.

The pulsed UV-excimer laser used as the photolysis/ablation source was a Lambda Physik EMG 103 MSC (248 nm). The excimer laser had a pulse duration of 15–20 ns (fwhm), and the cross section of the beam was varied with an iris of diameter of 2–4 mm, to give a homogeneous beam profile with suitable dimensions. A 0.5 ps UV-excimer laser was used as the ionization/detection laser at 248 nm. As was shown previously,[30,31] short UV-laser pulses considerably reduce the fragmentation in the mass spectra and sometimes avoid it completely.[36]

The laser ionization time-of-flight mass spectrometer, and its use for the detection of photoproducts under collision-free conditions, have previously been described in detail.[31,41,42] For vapor phase experiments, the photolysis laser and ionization laser were aligned collinear and opposing counterpropagating. The delay between photolysis and ionization was set at 4.2 μs. Spectra were taken as the average of 250 laser shots and data were taken at two pressures of the cube. For ablation experiments, the ablation laser was oriented first at a 45° angle and then perpendicular to the sample surface. The sample was placed 2–3 cm below the ionization laser aligned parallel to the surface. The delay between the ablation and the ionization was 200 μs. Spectra were taken as the average of 50 laser shots, exposing the same spot on the sample surface.

Acknowledgment. Financial support for this work was provided by the Office of Naval Research and the National Science Foundation (A.R.B.), the Bundesministerium für Forschung und Technologie BMFT 13N6159 (M.S.), and the Science and Engineering Research Council (SERC) (D.W.H.R.).

Registry Number supplied by authors. [(ᵗBu)GaS]₄, 135283-83-9.

OM940695A

(41) Zhang, Y.; Stuke, M. *Chemtronics* **1988**, *3*, 230.
(42) Grady, A. S.; Mapplebeck, A. L.; Russell, D. K.; Taylorson, M. G. *J. Chem. Soc., Chem. Commun.* **1990**, 929.